Regional Overview and Significance of the Mineralogy of the Upper Cretaceous Austin Chalk Group, Onshore Gulf of Mexico

Robert G. Loucks[1], Josh R. Lambert[1], Kim Patty[2],
Toti E. Larson[1], Robert M. Reed[1], and Christopher K. Zahm[1]

[1]*Bureau of Economic Geology, Jackson School of Geosciences,
University of Texas at Austin, University Station, Box X, Austin, Texas 78713–8924, U.S.A.*

[2]*Chesapeake Energy Corporation, Oklahoma City, Oklahoma 73154–0496, U.S.A.*

ABSTRACT

The Austin Chalk Group is an active exploration and exploitation target along the onshore Gulf of Mexico. Though it is considered a fractured reservoir play, it probably has late production from the chalk matrix. Development of natural and induced fractures as well as matrix pore characteristics of the argillaceous chalk are dependent on the mineralogy of the matrix. Therefore, it is important to know and understand the mineralogy of the Austin Chalk both stratigraphically and regionally along the onshore Gulf of Mexico. Based on 715 X–ray diffraction (XRD) analyses, the Austin Chalk mineralogy appears to have resulted from two populations of sediments: one related to a mixing trend between carbonate and siliciclastic minerals and the other related to the presence of fresh and altered volcanics. Dominant mineralogies are calcite, mixed-layer clays, and illite/mica. Quartz and feldspar are relatively less abundant. Calcite is related primarily to biological activity, clay minerals to terrigenous input and volcanism, and quartz and feldspar predominantly to volcanism. We propose that the mineral composition mixing trend(s) are controlled by biogenic carbonate production rate differences over time, which in turn are controlled by seawater chemistry. The siliciclastic component, which is postulated to be controlled by eolian processes, is hypothesized to have remained relatively constant for any particular well location (from the Texas-Mexico border to central Louisiana), and carbonate productivity either diluted the siliciclastic component (increasing biogenic productivity) or enhanced its abundance (reducing biogenic productivity). This large database of 715 XRD analyses produces a solid understanding of the regional and vertical stratigraphic distributions of the mineralogy of the Austin Chalk Group.

INTRODUCTION

The Upper Cretaceous Austin Chalk is considered a fractured reservoir play, but it is likely a mixed fracture/matrix play (Loucks et al., in press). Matrix pore characteristics and natural and induced fracture development of the argillaceous chalk depend on the mineralogy of the matrix. Therefore, it is important to know and understand the mineralogy of the Austin Chalk both vertically through the section and regionally along the onshore Gulf of Mexico. The objectives of this investigation are to define (1) the origin and abundance of mineral types, (2) general lithofacies (controls on grouping of minerals), (3) mineralogical trends both vertically through the Austin Chalk section and regionally

from the Texas-Mexico border to central Louisiana, and (4) controls on the variability of the mineralogy in the Austin Chalk.

This investigation is based on the description and analysis of 20 cores (cored intervals covering, in whole or in part, the entire Austin Chalk section) (Figs. 1 and 2), numerous associated petrographic thin sections, scanning electron microscope images, and 715 X–ray diffraction (XRD) analyses. In general, carbonate (predominantly calcite) (82%), clay minerals (11%), and quartz+feldspar (7%) compose the Austin Chalk. The variability of mineralogy follows a relatively well-defined mixing trend between carbonate and siliciclastic minerals (Fig. 3B). The mixing trend is consistent along the onshore Gulf of Mexico, suggesting that it is controlled by ocean chemistry rather than terrigenous input.

This regional overview of mineralogy not only provides an understanding of the depositional parameters relative to terrigenous input and ocean biological productivity, but also provides data that can be used to understand the range of mechanical properties and pore types during burial history (i.e., thermal history) of the Austin Chalk Group.

Figure 1. General stratigraphic section. Ages are from Phelps et al. (2013).

DATA AND METHODS

Rock data for this investigation comes from 20 cores (Table 1) distributed along the onshore Gulf of Mexico from the Texas-Mexico border to central Louisiana (Fig. 2). The well shown in Dimmit County, Texas (Fig. 2), is proprietary; the name and location are not listed, and the data from this well is not used in all analyses. All sections of the Austin Chalk were recovered in core, but only a few cores have complete or nearly complete sections. One of the wells with a complete cored section is the Getty 1 Lloyd Hurt well in La Salle County, Texas (Fig. 2), which is the type-cored well for the Austin Chalk in South Texas (Loucks et al., in press). Numerous thin sections were used to define meso- to megascale depositional and diagenetic features. Each thin section was impregnated with blue epoxy to highlight macropores and with blue fluorescent dye to highlight nanopores and micropores (using mercury-vapor light).

Selected samples from many of the wells covering all dominant lithofacies were viewed on a field-emission scanning electron microscope (FESEM) with an energy-dispersive X–ray spectrometer (EDS) to characterize biotas, mineralogy, crystal morphology, diagenetic features, and pores at their microscale of resolution. Ar–ion milled samples (see Loucks et al. [2009] for review) provide a flat surface that allowed high-resolution, two-dimensional analysis with EDS. The samples were observed using a FEI Nova NanoSEM 430 with dual Bruker XFlash EDS detectors at the University of Texas at Austin. Moderate accelerating voltages (10 to 15 kV) were generally used on these samples to prevent beam damage while still allowing EDS mapping; working distances were 3 to 10 mm.

XRD analysis was completed on 715 samples by three companies, including Weatherford Laboratories (now Stratum Reservoir), Chesapeake Energy Corporation, and Qmineral Analysis & Consulting. The samples were analyzed for bulk analysis, which provided percentages of major minerals and semiquantitative analysis of clay minerals. Mineral mean values are provided in Table 2. Individual minerals are listed by percentage of the whole rock, whereas framework-composition types (carbonate, clay minerals, and quartz+feldspar) are listed by percentage of framework composition. The mineralogic data was plotted using a chalk classification developed by Loucks et al. (in press) that emphasizes the apparent mixing trend of carbonate and siliciclastic minerals.

REGIONAL GEOLOGIC SETTING AND GENERAL STRATIGRAPHY

The Austin Chalk Group (Coniacian to lower Campanian) is one of several chalks that were deposited on the drowned Lower Cretaceous paleoshelf during a worldwide relative sea-level rise (Phelps et al., 2013). It overlies the Eagle Ford Group and underlies the Taylor Group (Fig. 1). The drowned shelf at the time of Austin Chalk deposition had regional topographic variations (Fig. 2) that controlled water depths, regional and vertical variations in lithofacies, and source-rock quality (Loucks et al., in press). Thicker sections of the Austin Chalk were deposited in the Maverick Basin, East Texas Basin, and North Louisiana Salt Basin, and thinner sections were deposited over the San Marcos Arch and Sabine Uplift, (Fig. 2). See Dennen and Hackley (2011, their figure 5) for a detailed map of these paleogeographic features.

The Austin Chalk strata in the area of investigation was deposited in relatively deeper water throughout. Loucks et al. (in press) suggested that it was deposited on the outer shelf below the storm wave base. Referencing the depth of the storm wave base in the present Gulf of Mexico (Reading and Collinson, 1996), Austin Chalk water depths are estimated to have been deeper than 300 ft (100 m). The biota in the Austin Chalk also reflect more open marine conditions in the shallow-water column. Planktic biota includes planktic foraminifera, calcispheres, and coccolithophores (Loucks et al., in press). Lesser benthic biota includes inoceramid clams, oysters and other thin-shelled mollusks, and echinoid fragments. Highly burrowed (predominantly horizontal), organic-matter-lean layers alternate with laminated, organic-matter-rich layers are a distinct feature of the Austin Chalk's lower half. These alternating beds signify that the bottom waters and sediment varied between aerobic and anaerobic conditions. These aerobic-to-anaerobic cycles were postulated by Loucks et al. (in press) to be Milankovitch cycles similar to those reported for the age-equivalent Niobrara Chalk in the Western Interior Seaway (Locklair and Sageman, 2008).

A series of volcanic features (Uvalde and Travis volcanic fields) occurs in the northern area (landward) of the Austin Chalk in Central and south-central Texas (Fig. 2) (Baldwin and Adams, 1971; Barker and Young, 1979; Ewing and Caran, 1982; Miggins et al., 2002; Griffin et al, 2010; Pierce et al., 2016). Griffin et al. (2010) defined two distinct phases of magmatic activity: the earlier intrusions were emplaced 84.1 to 81.5 Ma ago, and the later intrusions were emplaced 78.8 to 76.2 Ma ago. The older intrusions would be contemporaneous with the deposition of upper Austin Chalk strata, and some volcanic beds and debris are recognizable in the Austin Chalk cores. Pierce et al. (2016) provided ash-bed dates for the Eagle Ford Group. Some of the ash beds were dated as early Coniacian (87.1 Ma), suggesting that some regional volcanism may have been active during lower Austin Chalk deposition. However, it must be noted that not all of the volcanic features shown in Figure 2 have exact age dates associated with them.

OVERVIEW OF MINERALOGY

The 715 XRD data points are plotted on a ternary mineralogy diagram that has carbonate, clay minerals, and quartz+feldspar (Fig. 3A) as end-members. Several distinct trends are apparent on the ternary mineralogy diagram. The most prominent trend is a distribution of data points lying between the carbonate end-member and the clay-mineral end-member (Fig. 3B). As will be shown later, this major trend may actually have two subtrends, as displayed by a separation of data at the end denoting high clay content. This trend line appears to be a mixing line between carbonate and clay mineral–rich siliciclastic material. Also, when data from individual wells were viewed, the mineralogy trend
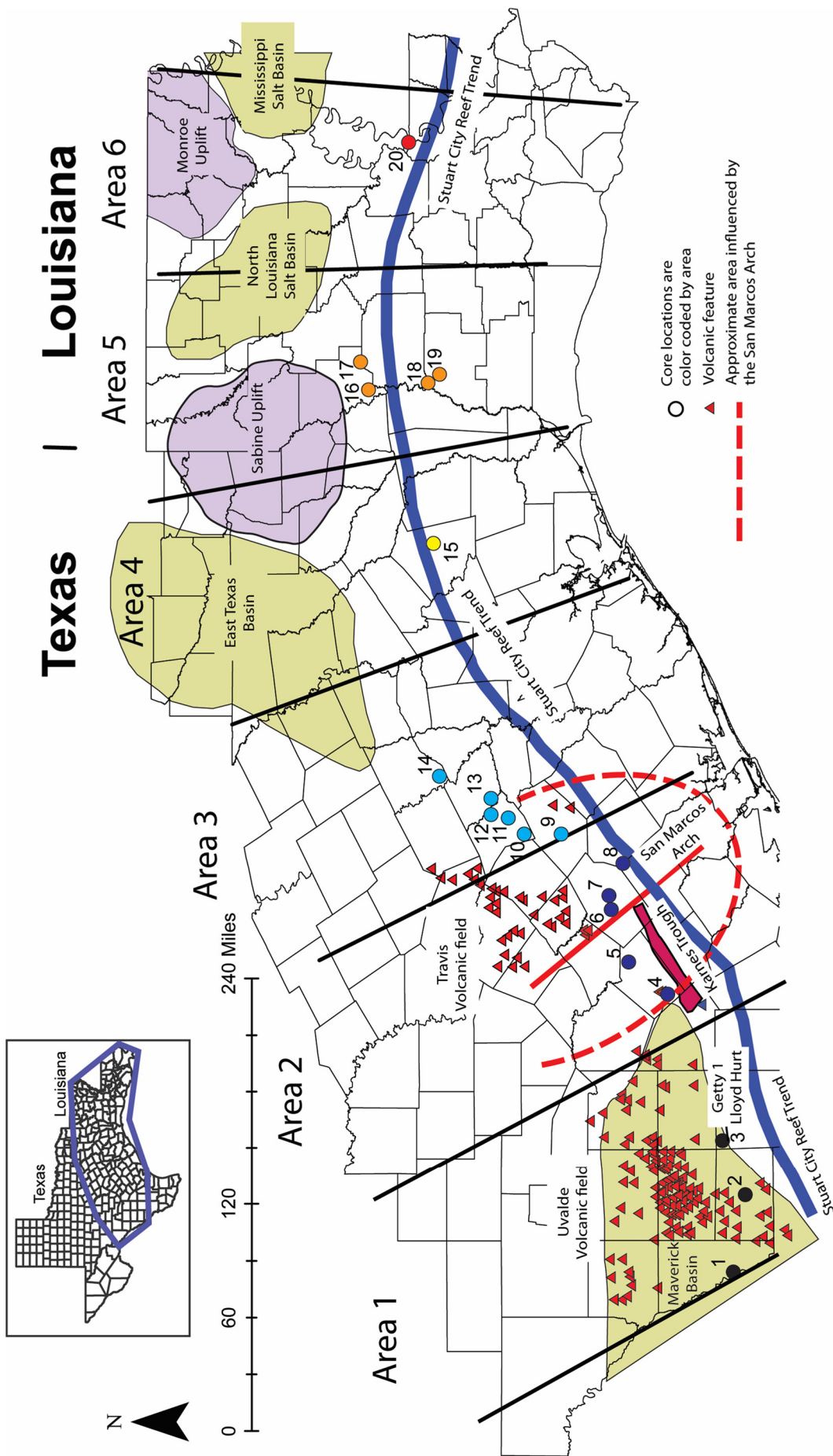
Figure 2. Locations of the wells used in this investigation. Wells are numbered and identified in **Table 1**. The outlines of the East Texas Basin, North Louisiana Salt Basin, and Mississippian Salt Basin are from Dennen and Hackley (2012). A number of volcanic features are shown with red triangles according to Baker and Young (1979) and Ewing and Caran (1982). There are not enough data provided in the literature to define the age of the volcanic features relative to Austin Chalk deposition. The area of investigation is divided into six geographic areas. The type-cored section in the Getty Lloyd Hurt well for the Austin Chalk is located in La Salle County, Texas.
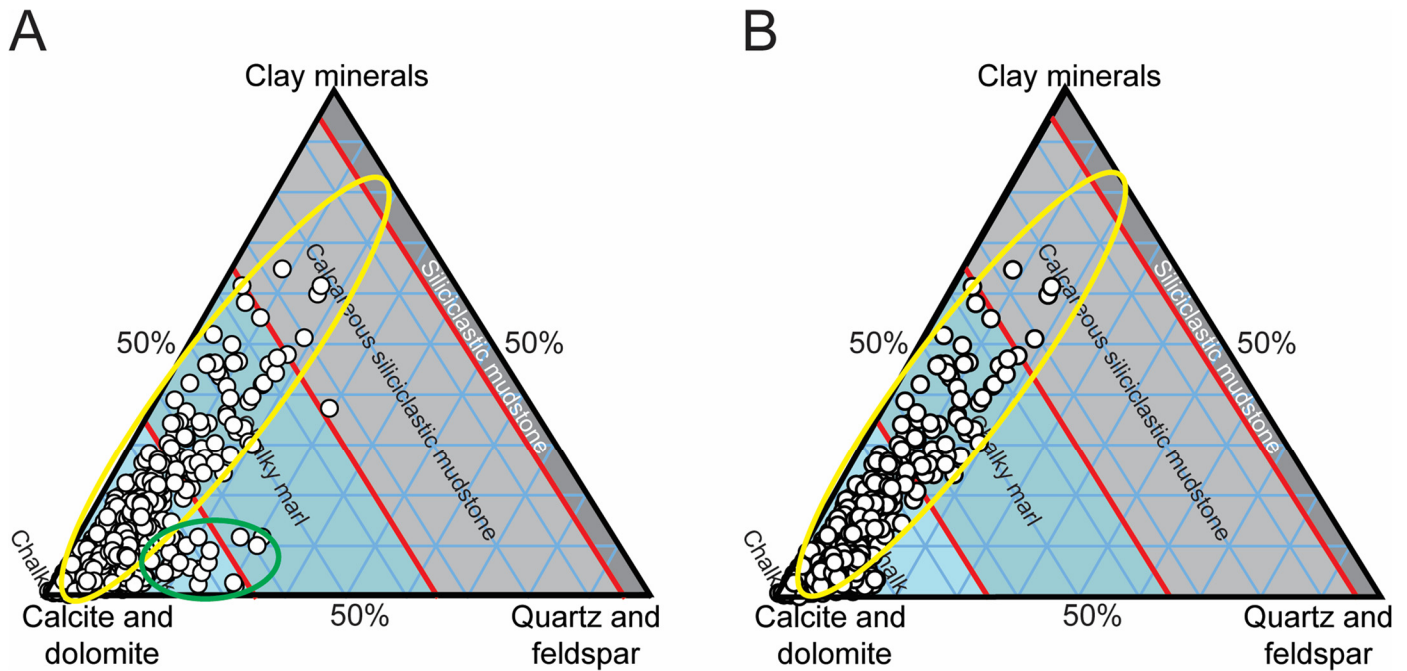
A

B

Figure 3. Ternary mineralogic diagrams. (A) Ternary diagram of all samples (715 X–ray diffraction analyses). The general trend of the data is shown by a yellow ellipse. A green ellipse outlines samples associated with Austin Chalk debrites containing volcanic-related minerals such as quartz and feldspar. Much of the volcanic-rich samples are from the upper Austin Chalk in the Trans Ocean 1 Orts, Getty 1 Lloyd Hurt cores, and the proprietary well. (B) Ternary diagram of all samples without the volcanic rich-samples.

Table 1. List of cores and associated information including number of samples per well. ID corresponds to the core number designation in Figure 2. The proprietary core is plotted in the center of Dimmit County as the exact location cannot be shown.

ID	Well name	API#	County/Parish	Number of samples
1	Strata–X 1 Cinco Saus Creek	42323334530000	Maverick Co., TX	14
2	Proprietary core		Dimmit Co., TX	113
3	Getty Oil 1 Lloyd Hurt	42283303050000	La Salle Co., TX	24
4	Tesoro Petroleum 1 Valcher	42493302300000	Wilson Co., TX	14
5	Prairie Producing 1 Brechtel	42493700257600	Wilson Co., TX	3
6	Evergreen Oil 1 Vicker Olyn	42177308050000	Gonzales Co., TX	52
7	Trans Ocean Oil 2 HP Orts	42177302030000	Gonzales Co., TX	113
8	Devon Energy 1 Medina	42123338730000	Dewitt Co., TX	16
9	Cities Service 1–B Ivy	42149305680000	Fayette Co., TX	4
10	Prairie Producing 1 Schautschick	42287300470000	Lee Co., TX	27
11	Prairie Producing 1 J A Smelley	42287300480000	Lee Co., TX	55
12	Prairie Producing 1 Marburger	42287000000000	Lee Co., TX	69
13	Champlin Petroleum 1 Brinkman Lancier	42051306030000	Burleson Co., TX	14
14	Prairie Producing 1 Frances Restino	42395300350000	Robertson Co., TX	7
15	Shell 1 Southern Paper Mills	42373000180000	Polk Co., TX	11
16	Stonegate Production 1 Donner	17085220990000	Sabine Ph., LA	33
17	Coffman 1 Cabra	17085207510000	Sabine Ph., LA	18
18	ARCO 1 W Singletary	17011206160000	Beauregard Ph., LA	32
19	Cortex Energy C1 Musser Davis	17011203250000	Beauregard Ph., LA	14
20	Marathon Oil 1 Robert Todd	17125200260000	West Feliciana Ph., LA	56

Table 2. Mean mineralogy and standard deviation by lithofacies.

Lithofacies	Mean	Std. Dev.	Lithofacies	Mean	Std. Dev.
% calcite all lithofacies	80.4	13.7	% mixed-layer clay all lithofacies	5.5	6.5
% calcite lithofacies 1	87.6	7.5	% mixed-layer clay lithofacies 1	2.4	1.6
% calcite lithofacies 2	76.9	15.1	% mixed-layer clay lithofacies 2	7.0	7.4
% calcite lithofacies 3	78.1	11.3	% mixed-layer clay lithofacies 3	6.8	7.9
% calcite lithofacies 4	70.2	18.7	% mixed-layer clay lithofacies 4	9.8	10.3
% dolomite all lithofacies	0.8	1.0	% illite/mica all lithofacies	3.2	7.6
% dolomite lithofacies 1	0.7	0.7	% illite/mica lithofacies 1	1.3	0.8
% dolomite lithofacies 2	0.7	1.0	% illite/mica lithofacies 2	3.6	7.5
% dolomite lithofacies 3	0.6	1.0	% illite/mica lithofacies 3	3.6	6.7
% dolomite lithofacies 4	0.4	0.9	% illite/mica lithofacies 4	8.2	19.3
% quartz all lithofacies	4.0	2.3	% chlorite all lithofacies	0.6	1.7
% quartz lithofacies 1	3.9	2.2	% chlorite lithofacies 1	0.3	0.4
% quartz lithofacies 2	4.5	2.5	% chlorite lithofacies 2	0.8	1.8
% quartz lithofacies 3	3.5	1.5	% chlorite lithofacies 3	1.3	4.5
% quartz lithofacies 4	3.6	1.7	% chlorite lithofacies 4	0.8	1.0
% plagioclase all lithofacies	2.2	1.6	% kaolinite all lithofacies	0.7	1.8
% plagioclase lithofacies 1	2.0	1.1	% kaolinite lithofacies 1	0.2	0.6
% plagioclase lithofacies 2	2.4	1.7	% kaolinite lithofacies 2	1.0	2.0
% plagioclase lithofacies 3	2.2	1.9	% kaolinite lithofacies 3	1.5	3.4
% plagioclase lithofacies 4	2.6	2.1	% kaolinite lithofacies 4	1.4	2.8
% K-feldspar all lithofacies	0.	0.4	% apatite all lithofacies	0.3	0.5
% K-feldspar lithofacies 1	0.1	0.1	% apatite lithofacies 1	0.3	0.2
% K-feldspar lithofacies 2	0.2	0.5	% apatite lithofacies 2	0.3	0.6
% K-feldsparl ithofacies 3	0.1	0.3	% apatite lithofacies 3	0.4	0.6
% K-feldspar lithofacies 4	0.4	0.8	% apatite lithofacies 4	0.4	0.5
			% pyrite all lithofacies	0.9	1.2
			% pyrite lithofacies 1	0.3	0.4
			% pyrite lithofacies 2	1.2	1.4
			% pyrite lithofacies 3	1.4	1.2
			% pyrite lithofacies 4	2.1	1.7

lines are shown to be much more distinct by well; this will also be discussed in a later section.

A second trend plots from the carbonate end-member toward the quartz+feldspar end-member. Not all wells show this second trend. This trend can be interpreted as the result of material possibly transported from shallower updip areas or as original sediment containing altered volcanic ash material. The latter explanation corresponds to the presence of Austin Chalk–age volcanic intrusions (Fig. 2).

Histogram and cumulative frequency plots of mineralogy show the ranges of percent values for each end-member (Fig. 4). Carbonate shows the widest range in values, with clay minerals showing a similarly wide range and quartz plus feldspar showing the narrowest (see Fig. 4 for the ranges of values). Here it is important to note that Austin Chalk samples have a broad range of clay-mineral abundance (Fig. 4B), which will have a strong effect on rock mechanics by lowering unconfined compressive strength as clay abundance increases. Figure 4D shows the relatively smooth trend of mixing between carbonate and siliciclastic material.

The cross-plot (all samples) of carbonate versus clay minerals and carbonate versus quartz plus feldspar distinctly shows the two major mineralogy trends (Fig. 5A). The carbonate versus clay minerals cross-plot (Fig. 5B) displays a relatively tight relationship that starts near 0% clay and projects toward 80% clay. These XRD samples are from 20 wells with a spatial distribution of approximately 600 mi (1000 km) (Fig. 2) and covering the complete Austin Chalk stratigraphic section. The trend indicates

that there must be a broad, common regional control over this mixing between carbonate and clay minerals. Local sediment input does not appear to control the mineralogy mixing trend. A discussion on the possible controlling mechanism of these two mineral composition end-members is presented later.

Though the carbonate versus quartz plus feldspar trend (Fig. 5C) is not as well defined as the carbonate versus clay mineral trend, it does displays two rough trends. A weak trend line can be drawn that starts near 0% quartz+feldspar and trends toward 20% quartz+feldspar. A second weak trend line can be drawn starting near 0% quartz+feldspar and trending toward 80% quartz quartz+feldspar. The clay mineral to quartz-feldspar plot (Fig. 5D) illustrates two very weak trends. One trend extends along the clay-mineral axis and a secondary trend is noted that runs along the quartz-feldspar axis. These cross plots emphasize that the general siliciclastic ratio of clay minerals to quartz+feldspar is approximately 80 to 20%, respectively.

CHARACTERISTICS AND ORIGINS OF INDIVIDUAL MINERAL TYPES

Table 2 summarizes the mean values of individual mineral abundances in the Austin Chalk by total sample analysis and by lithofacies. A short characterization of each mineral is provided in this section. A series of SEM EDS images (Fig. 6) of the minerals and thin-section microphotographs (Fig. 7) are shown. Because of the dominant clay- to fine-silt-sized grains, the samples

Figure 4. Histograms of mineral end-members. (A) Histogram of carbonate minerals, which are dominated by calcite. (B) Histogram of clay minerals. (C) Histogram of quartz+feldspar. (D) Histogram of carbonate and siliciclastics showing the relatively smooth transitions between the two major end-members.

were imaged at the SEM scale to resolve individual minerals as well as their texture and fabric.

Calcite: Calcite is the dominant mineral, making up 80% (mean bulk) of the whole rock (Table 2). Most of the calcite is from biological components such as coccolithophores (preserved as coccolith elements), planktic foraminifera, and calcispheres (Fig. 6). Other lesser biologic allochems are benthic foraminifera, mollusks, and echinoderms. Coccolith elements are the most abundant component and dominate the matrix. Some calcite is diagenetic, resulting mainly from pressure solution of allochems (Fig. 7A). The dissolved calcite recrystallizes as cement fill in intraparticle pores in fossils, especially foraminifera (Fig. 7A). It is also an abundant interparticle cement that constitutes the major lithification process of the chalk (Fabricius, 2007; this study).

Dolomite: Dolomite composes less than 0.8% of the chalk on average (Table 2). It occurs as Fe–rich, zoned, very fine euhedral crystals (Figs. 6C–6E). Some dolomite crystals appear to be abraded (Fig. 6D) and may be detrital in origin.

Quartz: Quartz generally occurs as clay- to fine-silt-sized grains (Fig. 6). It is approximately 4% (mean bulk) of the whole rock (Table 2). Quartz grains may originate from weathering in subaerially exposed areas, from volcanic ash fallout, and/or from alteration of volcanic sediment. A minor amount of quartz is from the dissolution of radiolarians, which occur in small amounts in the Austin Chalk. Much of the quartz is clay to silt sized, possibly suggesting eolian dust deposition. The volcanic quartz, where it occurs with volcanic feldspar, is angular, commonly tabular, and very clear (Fig. 7C and 7D). Much of the volcanic quartz appears to be contained in the upper Austin Chalk and west of the East Texas Basin. These South and Central Texas areas have many volcanic features (Fig. 2) but generally have been described as having a silica-poor composition (Barker and Young, 1979). Therefore, no exact source can be positively provided for the quartz volcanic components.

Plagioclase: Plagioclase makes up approximately 2.2% of the whole rock (Table 2). It generally ranges in size from very fine to fine silt (Fig. 6), with some medium-silt-sized particles (Fig. 6H). EDS analysis indicates that all the plagioclase observed is sodium-rich and albite. In some thin sections, it appears very fresh, angular, and twinned (Fig. 7D). It occurs along with the interpreted volcanic quartz and is also considered to be volcanic in origin. EDS analysis of a well-preserved Austin Chalk volcanic ash layer analyzed in this investigation displayed similar albite grains, indicating that albite is probably volcanic in origin.

K–feldspar: A very minor amount of K–feldspar is noted in the XRD analyses: 0.13% (mean bulk) of the whole rock volume. It is difficult to recognize in EDS maps as it is very fine and problematic to separate from illite that is also potassium-rich. Also, it may be present as incompletely albitized grains.

Mixed-layer clay: Mixed-layer clay (25 to 30% expandable layers) is a common clay type and makes up 5.5% (mean bulk) of the whole rock volume. Ten percent of the samples have a mean bulk of 15% or greater. Several samples are greater than 40% mixed-layer clay. SEM imaging shows the clay to have a platelet morphology. Clay forms matrices and peloids (probably marine snow) (e.g., Figs. 7C and 7F) within the chalk. In the Upper Cretaceous Eagle Ford Group in South Texas, Denne et al. (2014) attributed the origin of this clay type to altered volcanic ash deposited by eolian processes.
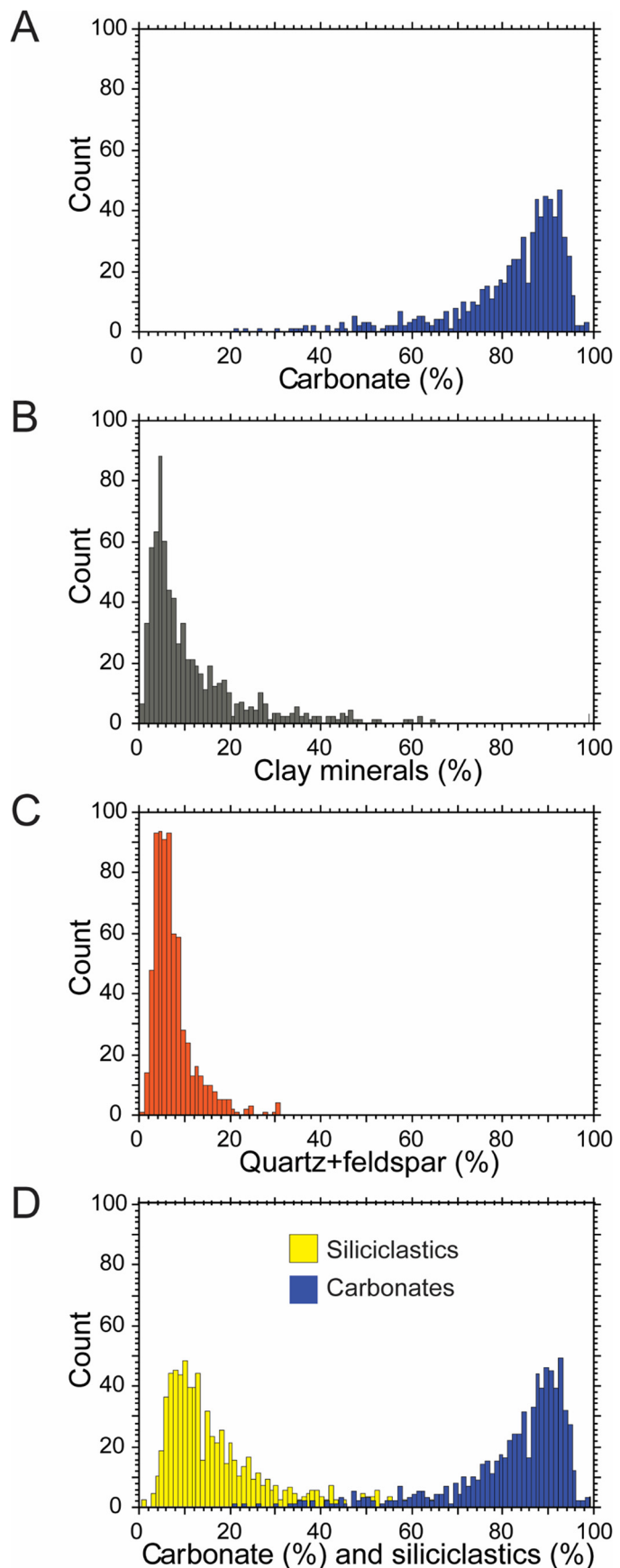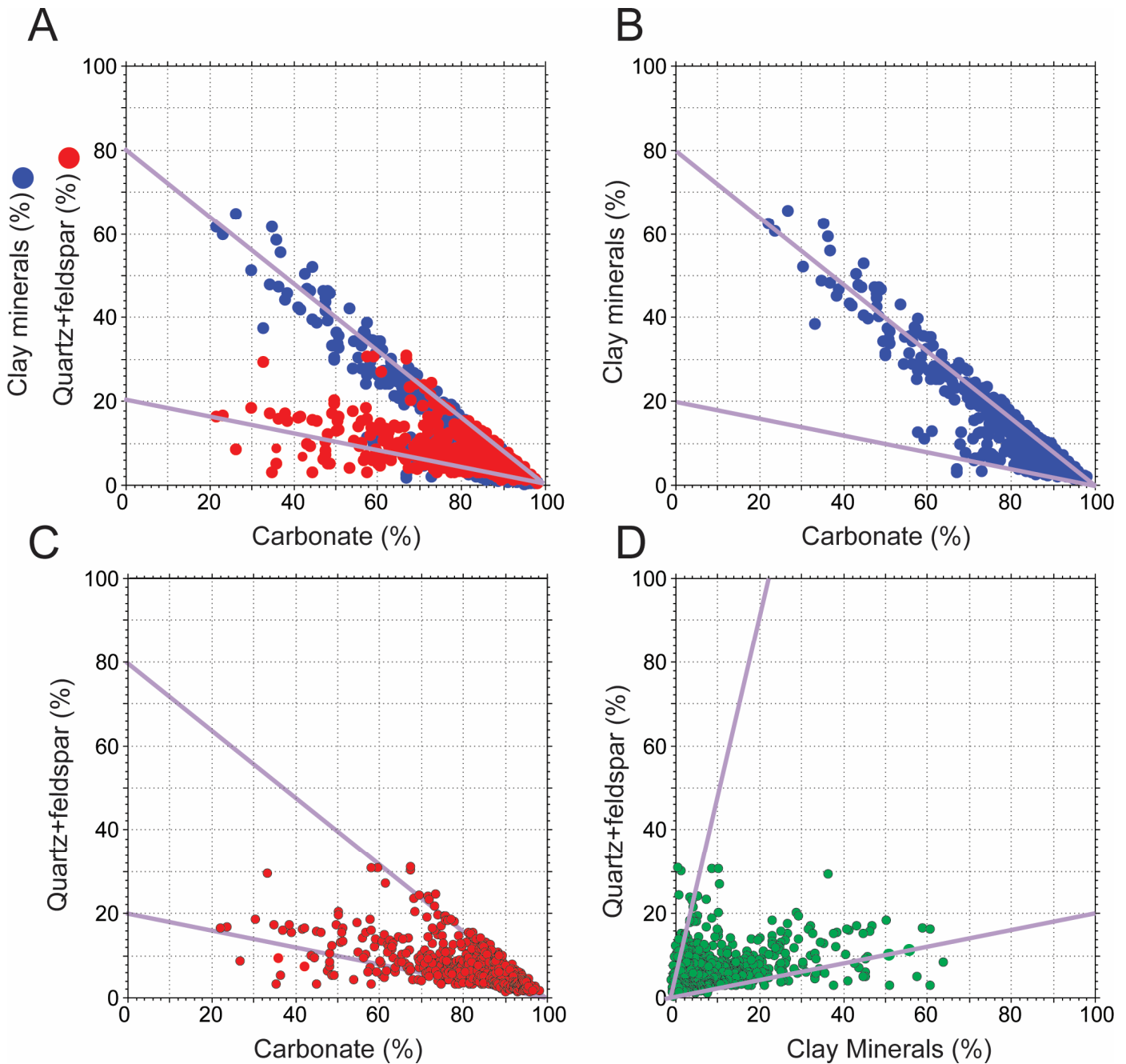
Figure 5. Mineral-ratio cross plots. (A) Combined plot of percentage of carbonate versus clay minerals and carbonate versus quartz+feldspar. The approximate ratio between clay minerals and quartz+feldspar is 80–20%. (B) Plot of percentage of carbonate versus clay minerals. The 0–80% trend is the dominant trend. (C) Plot of percentage of carbonate versus quartz+feldspar. The 0–20% trend is dominant, but the secondary trend of 0–80% is evident. (D) Plot of percentage of clay versus quartz+feldspar. Again, two trends are noted.

Illite/mica: Illite/mica is a common clay type (Figs. 6B, and 6F–6H), composing 3.3% (mean bulk) of the whole rock. The preponderance of samples is composed of less than 15% illite/mica, with only seven samples having bulk values over 15%. Illite/mica occurs in the matrix similarly to mixed-layer clay.

Chlorite: Chlorite is present as larger grains of clay (Fig. 7I) (a few tens of microns long) and makes up approximately 0.6% (mean bulk) of the rock volume. Four percent of the samples are between 3 to 6% chlorite. In the Austin Chalk volcanic ash layer mentioned earlier, larger chlorite grains were noted, suggesting that the chlorite is from volcanic ash beds.

Kaolinite: Kaolinite occurs in booklets in some samples and makes up 0.7% (mean bulk) of the rock volume. Three percent of the samples have 5% or greater amounts of kaolinite and 5 samples have 10% or greater amounts of kaolinite. Kaolinite can be an alteration product of volcanic ashes (Ece et al., 2003) or a diagenetic precipitate in larger intraparticle pores of foraminifera.

Apatite: Apatite generally occurs as fish detritus (e.g., Fig. 7E), but some occurrences of volcanic euhedral apatite (Fig. 6H) are present, similar to what Reed et al. (2019) noted. The bulk mean is approximately 0.3%.
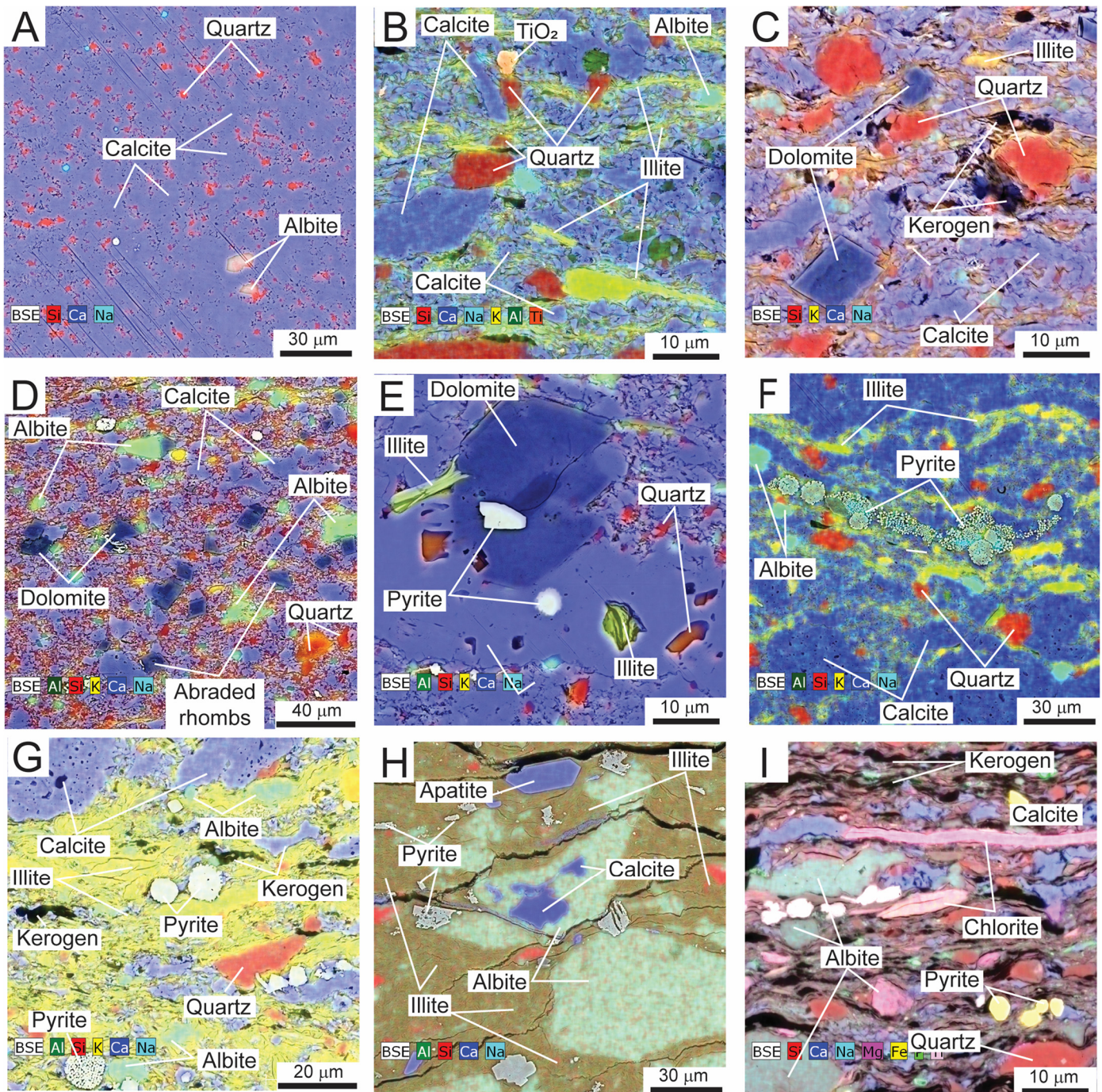
Figure 6. Scanning electron microscope energy-dispersive spectrometry images of samples. (A) Lithofacies 1. Sample dominated by calcite with minor albite silt and clay- to silt-sized quartz. Cities Service 1–B Ivy, 8427.7 ft (2570.8 m), Fayette County, TX. (B) Lithofacies 3. Laminated mixture of mineralogy. Numerous calcite particles of inoceramid fragments and coccolith elements. Abundant illite and some quartz silt. Marathon Oil 1 Robert Todd, 12,875.5 ft (3924.5 m), West Feliciana Parish, LA. (C) Lithofacies 2. Abundant calcite coccolith fragments. Some quartz silt and kerogen. Zoned dolomite is present and may be detrital with authigenic overgrowths. Getty Oil 1 Lloyd Hurt, 6732.8 ft (2052.2 m), La Salle County, TX. (D) Lithofacies 4. Mixture of calcite and dolomite grains. Some albite and quartz silt. Cities Service 1–B Ivy, 8410 ft (2563.4 m), Fayette County, TX. (E) Lithofacies 4. Authigenic dolomite replacing an inoceramid fragment. Pyrite replacing dolomite and calcite grains. Cities Service 1–B Ivy, 8311 ft (2533.2 m), Fayette County, TX. (F) Lithofacies 2. Sample dominated by calcite inoceramid grains with quartz and albite silt grains. A stringer of pyrite framboids is present as well as several seams of illite. Tesoro Petroleum 1 Valcher, 6720 ft (2048.3 m), Wilson County, TX. (G) Lithofacies 4. Sample has abundant illite, including calcite inoceramid grains. Common pyrite framboids and kerogen. Strata–X 1 Cinco Saus Creek, 3443.4 ft (1049.5 m), Maverick County, TX. (H) Lithofacies 4. Sample dominated by illite and silt- to very fine sand-sized grains of albite. Some albite is partly replaced by calcite and pyrite. A euhedral crystal of apatite is present. Devon Energy 1 Medina, 12,477.7 ft (3803.2 m), Dewitt County, TX. (I) Lithofacies 4. Laminated fabric with abundant organic microbial mats. Several large pieces of chlorite are present as well as albite silt. Prairie Producing 1 Marburger, 6977 ft, (2126.6 m), Lee County, TX.
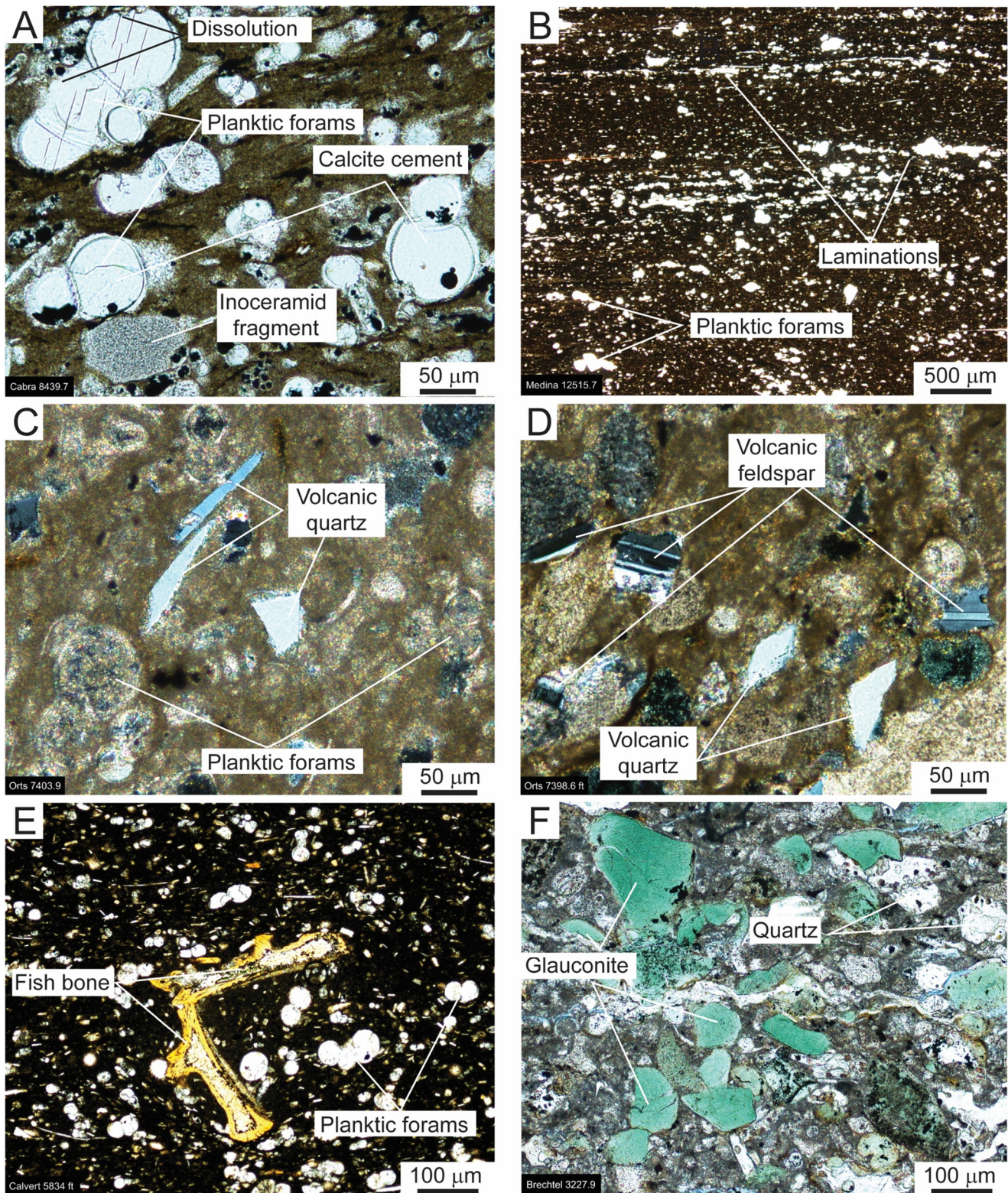
Figure 7. Thin-section examples of fabric and mineral types. (A) Burrowed planktic foraminifera chalky marl with an inoceramid fragment in a peloidal matrix of coccolith elements. The foraminifera display dissolution of tests, and the former intraparticle chambers are filled with calcite cement. Lithofacies 2. Coffman 1 Cabra, 8439 ft (2572.2 m), Sabine Parish, LA. **(B)** Laminated fabric with planktic foraminifera in a peloidal matrix of coccolith elements and clay minerals. Lithofacies 4. Devon Energy 1 Medina, 12,515.7 ft (3814.8 m), Dewitt County, TX. **(C)** Tabular and angular volcanic quartz in a peloidal planktic foraminifera marly chalk. Photomicrograph taken with cross-polarized light. Trans Ocean Oil 2 HP Orts, 7403 ft (2572.2 m), Gonzales, TX. **(D)** Volcanic-twinned plagioclase and volcanic quartz in a peloidal marly chalk matrix. Photomicrograph taken with cross-polarized light. Trans Ocean Oil 2 HP Orts, 7398 ft (2254.9 m), Gonzales, TX. **(E)** Fish bone in a peloidal planktic foraminifera marly chalk. Tesoro 1 Calvert, 5834 ft (1778.2 m), Frio County, TX. **(F)** Very fine- to fine-sand-sized glauconite grains in a debris flow. Prairie Producing 1 Brechtel, 3227 ft (983.6 m), Wilson County, TX.

Pyrite: Pyrite is a common authigenic mineral in the Austin Chalk Group and occurs generally as pyrite framboids (Figs. 6F and 6G) and replacement products (Figs. 6E and 6H). It has a bulk mean volume of 0.9%, but 16.5% of the samples have a mean pyrite percentage between 2 and 8%. The pyrite, as will be discussed in more detail later, is strongly controlled by lithofacies (Table 2), with the organic-matter-rich laminated lithofacies having the most pyrite (mean 2.1%). This association with the organic-matter-rich laminated lithofacies supports the conclusion that the pyrite formed early in anaerobic bottom sediments (Raiswell and Canfield, 1998).

TiO$_2$: TiO$_2$ (probably rutile) occurs in most samples. It did not show up in the XRD analyses but is commonly seen as a trace mineral in EDS images (Fig. 6B). TiO$_2$ is generally considered to be of terrigenous origin (e.g., Robertson and Degnan, 1998). The clay- to very fine-silt-sized range of the grains suggests that the TiO$_2$ may have been deposited by eolian processes.

Glauconite: In the Austin Chalk B1 unit in South and Central Texas, glauconite is common in debrites (Fig. 7F) (Loucks et al., in press). Glauconite did not appear in the XRD analyses; it was presumably included with the clay minerals to which it has a similar chemical composition. The glauconite appears as rounded, very fine-sand-sized grains. Glauconite is a diagenetic mineral that can have several different origins (Triplehorn, 1965; Jeans et al., 1982), including a shallow-water marine setting (Chafetz and Reid, 2000). A shallow-water origin would fit well with glauconite in the Austin Chalk being transported from a shallower water area updip. Another origin postulated is the alteration of volcanic material in seawater (Jeans et al., 1982). This would fit with the occurrence of volcanic quartz, albite, and apatite.

GENERAL REGION-WIDE AUSTIN CHALK LITHOFACIES TYPES

The Austin Chalk strata along the onshore Gulf of Mexico can be divided into five general lithofacies (Fig. 8). Their mineralogies are somewhat distinct, though with some overlap (Loucks et al. in press). Table 2 provides the mean values of mineralogy for the four most prominent lithofacies. The matrix of each lithofacies is generally peloidal, coccolith-element-rich hash and clay minerals. The larger allochems are planktic and lesser benthic foraminifera, calcispheres, inoceramid and oyster fragments, thin-shelled mollusks, and echinoderm plates.

Lithofacies 1 is a highly bioturbated, organic-matter-poor marly chalk (Fig. 8A). It is generally very light gray. Mean framework-grain composition for this lithofacies is 89.4% calcite, 4.4% clay minerals, and 6.2% quartz+feldspar. The ternary plot in Figure 9A shows that lithofacies 1 samples generally have less than 20% siliciclastic material. Only a few samples plot in the pure chalk range (greater than 95% carbonate). Total organic carbon (TOC) is commonly less than 0.5% (Loucks et al., in press). The fabric ranges from totally bioturbated to well-defined burrow traces. Most burrows are horizontal, but some are vertical. Mean pyrite is 0.3%, lowest of all the lithofacies (Table 2). Loucks et al. (in press) interpreted this lithofacies as having been deposited in a deeper-water setting below storm wave base on a drowned shelf during periods of oxygenated bottom-water and sediment conditions.

Lithofacies 2 (Fig. 8B) is similar in appearance to lithofacies 1, but much more siliciclastic rich and, in places, organic-matter rich. It is generally medium to dark gray. It is a highly bioturbated, moderately organic-matter-rich marly chalk to chalky marl. Mean framework-grain composition is 77.8% calcite, 14.1% clay minerals, and 8.1% quartz+feldspar. The ternary plot in Figure 9B shows that lithofacies 2 samples have the broadest range of siliciclastic material: between a few percent to nearly 75%. Mean pyrite content is 1.2%, indicating some reducing conditions. Mean TOC is approximately 1% (Loucks et al., in press). The fabric shows abundant horizontal burrow traces.

Loucks et al. (in press) interpreted this lithofacies as having been deposited in a deeper-water shelf setting below storm wave base. The bottom conditions were relatively restricted, varying between mildly aerobic to anaerobic.

Lithofacies 3 (Fig. 8C) is a poorly to moderately laminated, sparsely bioturbated, organic-matter-rich marly chalk. Mean framework-grain composition is 80.5% calcite, 13.5% clay minerals, and 6.0% quartz+feldspar. The ternary plot in Figure 9C shows that lithofacies 3 samples display a range of siliciclastic material, but it is generally less than 40%. Some samples are calcite-rich with values near the pure chalk range. Mean pyrite is 1.4%, indicating reducing conditions. This lithofacies can be light to dark gray. TOC has an approximate mean range of 1.5 to 1.7% (Loucks et al., in press). The fabric is laminated, but the laminations are disrupted by few horizontal burrows. The depositional setting was interpreted by Loucks et al. (in press) to have been a deeper-water shelf setting below storm wave base, where the bottom conditions ranged from dysaerobic to anaerobic based on laminations, higher TOC content, and some bioturbation. However, periods of oxygenation allowed some bioturbation.

Lithofacies 4 (Fig. 8D) is a well-laminated, argillaceous, organic-matter-rich marly chalk. It can be light to dark gray. Mean framework-grain composition is 72.6% calcite, 20.3% clay minerals, and 7.1% quartz+feldspar. The ternary plot in Figure 9D shows that lithofacies 4 samples display a broad range of carbonate minerals varying from approximately 20 to 90%. Mean pyrite is 2.1%, indicating strong reducing conditions. This lithofacies is the most pyrite and TOC rich. Average TOC is approximately 2% (Loucks et al., in press). The fabric is well-laminated without traces of bioturbation. Lithofacies 4 is characterized by large (centimeters/inches-long) inoceramid fragments. In the other lithofacies, bioturbation disaggregated inoceramid shells into their individual cell fragments. Based on laminations, lack of burrows, and higher TOC content, the depositional setting was interpreted by Loucks et al. (in press) to have been a deeper-water shelf setting below storm wave base, where the bottom conditions were strictly anaerobic.

Lithofacies 5 (Fig. 8E) is most common in the upper part of the Austin Chalk section but also occurs as thin units in the lower Austin Chalk (Loucks et al., in press). This lithofacies was deposited by gravity-flow processes (debrites) that produced a different texture and fabric from the other lithofacies. The major rock type is a fossiliferous, clast-bearing lime floatstone. Some of lithofacies 5 is rich in glauconite grains in the upper Austin Chalk section. Intraclasts and lithoclasts are common. In some gravity flows, some carbonate grainstone is present. Altered volcanic rock fragments (former glass shards) as well as volcanic quartz and feldspar may be present in lithofacies 5. In the upper Austin Chalk, the debrites were transported from an updip area, and the mineralogy and biota proportions are different (contains more oysters, echinoderm fragments, and benthic foraminifera) from those seen in lithofacies 1–4 (Loucks et al., in press).

VERTICAL TREND ANALYSIS IN MINERALOGY

Lithofacies types are key to understanding the vertical distribution of minerology because mineralogy is generally related to lithofacies, as discussed above. Core samples from many of these wells show a repeatable vertical stacking pattern. Loucks et al. (in press) described a generalized stacking pattern. They noted a stacking pattern through the Austin Chalk that reflects changing environmental conditions vertically through the section. These conditions affected TOC preservation (source-rock quality), clay-mineral content (brittleness), and porosity magnitude (reservoir quality). This stacking pattern is seen in cores from the Texas-Mexico border to central Louisiana. Overall, there is a significant change in lithofacies up-section from the more organic-matter-rich laminated lithofacies 3 and 4 and the organic-rich

fraction of lithofacies 2 into less organic-matter-rich bioturbated lithofacies 1 and the organic-poor fraction of lithofacies 2. This upward decrease in organic matter suggests an upward change from dominantly anaerobic conditions to more aerobic conditions. This stacking pattern is not seen on the San Marcos Arch, where the organic-matter-rich argillaceous units of the Austin Chalk greatly thin or pinch out. This stacking pattern affects mineral distribution in that the dominance of laminated lithofacies 3 and 4 in the lower half of the Austin Chalk are associated with an increase in siliciclastic and pyrite content, and the dominance of the calcite-rich, burrowed lithofacies 1 in the upper Austin chalk is associated with an increase in calcite and a decrease in clay minerals. In core from South Texas and on the San Marcos Arch is an upper chalk zone designated as Austin Chalk B1 (Ewing, 2013). This is the zone that has abundant debrites containing abundant glauconite, volcanic quartz, and feldspar.

REGIONAL TREND ANALYSIS IN MINERALOGY

Figures 10 and 11 show individual ternary mineralogic plots for each core in this investigation where the samples in each core are grouped by lithofacies. The dataset that was used to compose these graphs eliminated the volcanic-material-rich zones so that the suggested mixing trends of the normal Austin Chalk sedimentation could be defined and compared. All plots show lithofacies 1 to be relatively poor in siliciclastic material and lithofacies 2, 3, and 4 to show a broad spread of siliciclastic content. "Eyeballed" best-fit trend lines were drawn through the data points.

The grouping of the trend lines is shown in Figure 12. Two populations of trend lines are apparent. One is more clay rich than the other. The more clay-rich trend lines lie in far East Texas and Louisiana, and the more quartz-feldspar-rich trend lines lie in the areas of the San Marcos Arch and the Maverick Basin (South Texas) (Fig. 2). The more quartz-feldspar-rich trend lines appear to be in the areas of volcanic features as shown in Figure 2. Therefore, the enhanced abundance of quartz+feldspar may be related to contemporaneous volcanism. However, as noted earlier by Barker and Young (1979), the volcanics in South and Central Texas were silica poor (i.e., no quartz).

SPECULATION ON THE ORIGIN OF MINERALOGIC TREND LINES IN THE AUSTIN CHALK

A striking feature of the ternary mineralogical diagrams is that the data fall along a relatively well-behaved trend line (Fig. 12). These apparent well-behaved trend lines occur in wells ranging from the Texas-Mexico border to central Louisiana and appear not to be affected by stratigraphic position in the Austin Chalk section.

The trend lines indicate there are two end-members or sediment types that are mixing in a consistent manner. The two end-members are carbonate (predominantly calcite) and siliciclastic sediment (clay mineral, quartz, and feldspar). Therefore, the trend lines are considered to be a mixing trend as one end member increases and the other decreases.

Because the trend lines are consistent (i.e., similar), the different siliciclastic source areas appear not to have had a significant effect on the mineral composition regionally. The two possible dominant terrigenous source areas, which were separated by the Wester Interior Seaway, would have been the Appalachia area to the north and the Laramidia area to the west (see Cobban and McKinney [2004] for paleographic map). Also, seeing that the general composition of the siliciclastic sediment remained relatively constant throughout the Austin Chalk section along the Gulf of Mexico, a depositional process must be invoked that explains this consistency. This siliciclastic consistency and the very fine-grain size of the siliciclastic material (clay to fine silt)

suggests an eolian distribution system. Wind-blown dust is a common depositional process that can distribute large amounts of sediment worldwide (Kok et al., 2012). This eolian process would be an effective mixing mechanism of the transported sediment. Denne et al. (2014) also invoked an eolian origin for the fine-grained siliciclastic sediment in the underlying Upper Eagle Ford Group in South Texas. Also, some of the eolian dust was probably volcanic in origin.

As mentioned earlier, the major process for carbonate production was biological, mainly planktic organisms. The planktic organisms would be dependent upon regional ocean chemistry. As the regional ocean chemistry changed, the productivity of the organisms would change and hence their production volume also. It is beyond the objectives of this present investigation to define the detailed chemistry of the Gulf of Mexico waters during Austin Chalk time; however, we suggest it was probably changing ocean chemistry that controlled the mixing line by controlling the production volume of planktic organisms. This would mean siliciclastic input remained relatively constant over time, whereas the carbonate productivity varied.

CONCLUSIONS

The Austin Chalk Group is predominantly composed of calcite and clay minerals with lesser amounts of quartz and feldspar. The calcite is related to biological productivity, with most of it coming from planktic organisms such as coccolithophores, planktic foraminifera, and calcispheres. Other lesser biologic sources are mollusks and echinoderms. Coccolith elements are the most abundant component and dominate the matrix. Clay minerals, quartz, and feldspar may have been sourced in part by terrigenous eolian deposition or by volcanic ash fallout.

Based on 715 X–ray diffraction analyses, the Austin Chalk appears to have two populations of sediments: one related to a mixing trend (Fig. 3) between carbonate and siliciclastic minerals and the other related to altered volcanic-mineral-enhanced zones. The mixing trend (Fig. 3) runs parallel to the carbonate-clay mineral axis, indicating mixing between carbonates and siliciclastic sediments. This mixing trend appears to have two distinct subtrends (Fig. 3), with one that is enriched with quartz and feldspar. The enriched quartz and feldspar subtrend relates to sample locations in the areas of the San Marcos Arch and South Texas Maverick Basin, whereas the other subtrend relates to sample locations in far East Texas and Louisiana. The quartz and feldspar subtrend wells are associated with Upper Cretaceous aged volcanics; however, these volcanics have been analyzed and found to be silica poor. Therefore, these volcanics may not be the primary source of quartz and feldspar in the subtrend. Distant volcanism (western Mexico?) may have supplied a portion of the volcanic sediment.

Regarding the observed mixing between carbonates and siliciclastics, we suggest it was probably changing ocean chemistry that controlled the mixing line by controlling the production volume of planktic organisms. This would mean that the siliciclastic input remained relatively constant over time and the carbonate productivity varied. A detailed chemical analysis of the paleo-oceanography is needed to substantiate this proposed mechanism. However, our proposed mixing mechanism provides a starting point for further investigations.

ACKNOWLEDGMENTS
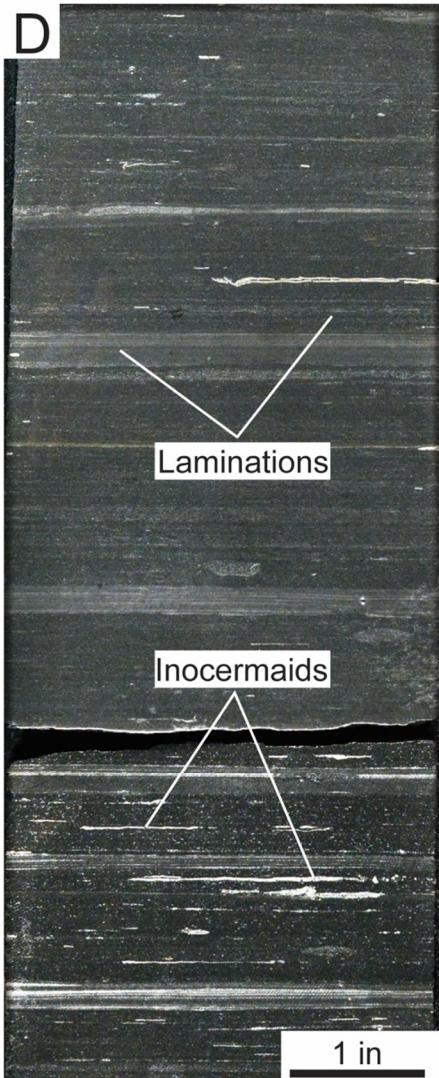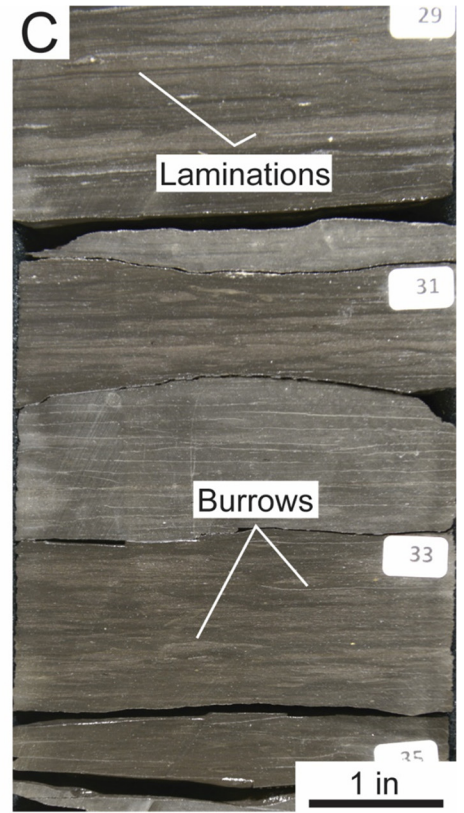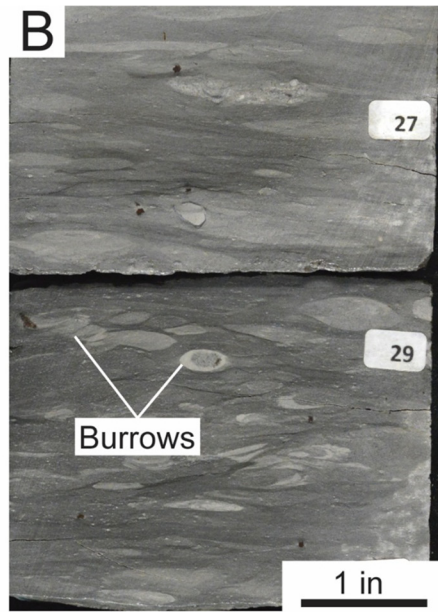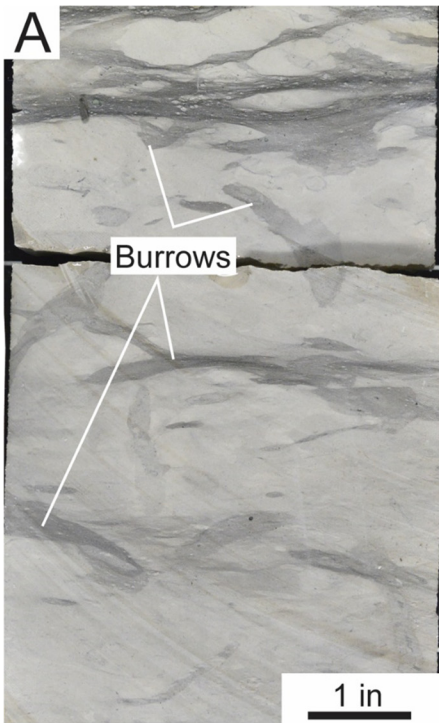
(**FACING PAGE**) **Figure 8. Examples of Austin Chalk lithofacies. (A) Lithofacies 1 is a highly bioturbated, organic-matter-poor marly chalk (a few are true chalks). Tesoro 1 Calvert, 6202 ft (1890.4 m), Frio County, TX. (B) Lithofacies 2 is a highly bioturbated, moderately organic-matter-rich, very argillaceous marly chalk to chalky marl. Prairie Producing 1 Brechtel, 3271 ft (997.0 m), Wilson County, TX. (C) Lithofacies 3 is generally a poorly to moderately laminated, sparsely bioturbated, organic-matter-rich, argillaceous to very argillaceous marly chalk. Marathon Oil 1 Robert Todd, 12,985 ft (3957.8 m), West Feliciana Parish, LA. (D) Lithofacies 4 is a well-laminated, argillaceous, organic-matter-rich marly chalk to chalky marl. Devon Energy 1 Medina 12,544 ft (3823.4 m), Dewitt County, TX. (E) Lithofacies 5 is a fossiliferous, clast-bearing, commonly glauconite-grain-rich lime floatstone. Prairie Producing 1 Brechtel, 3254 ft (1074.1 m), Wilson County, TX.**
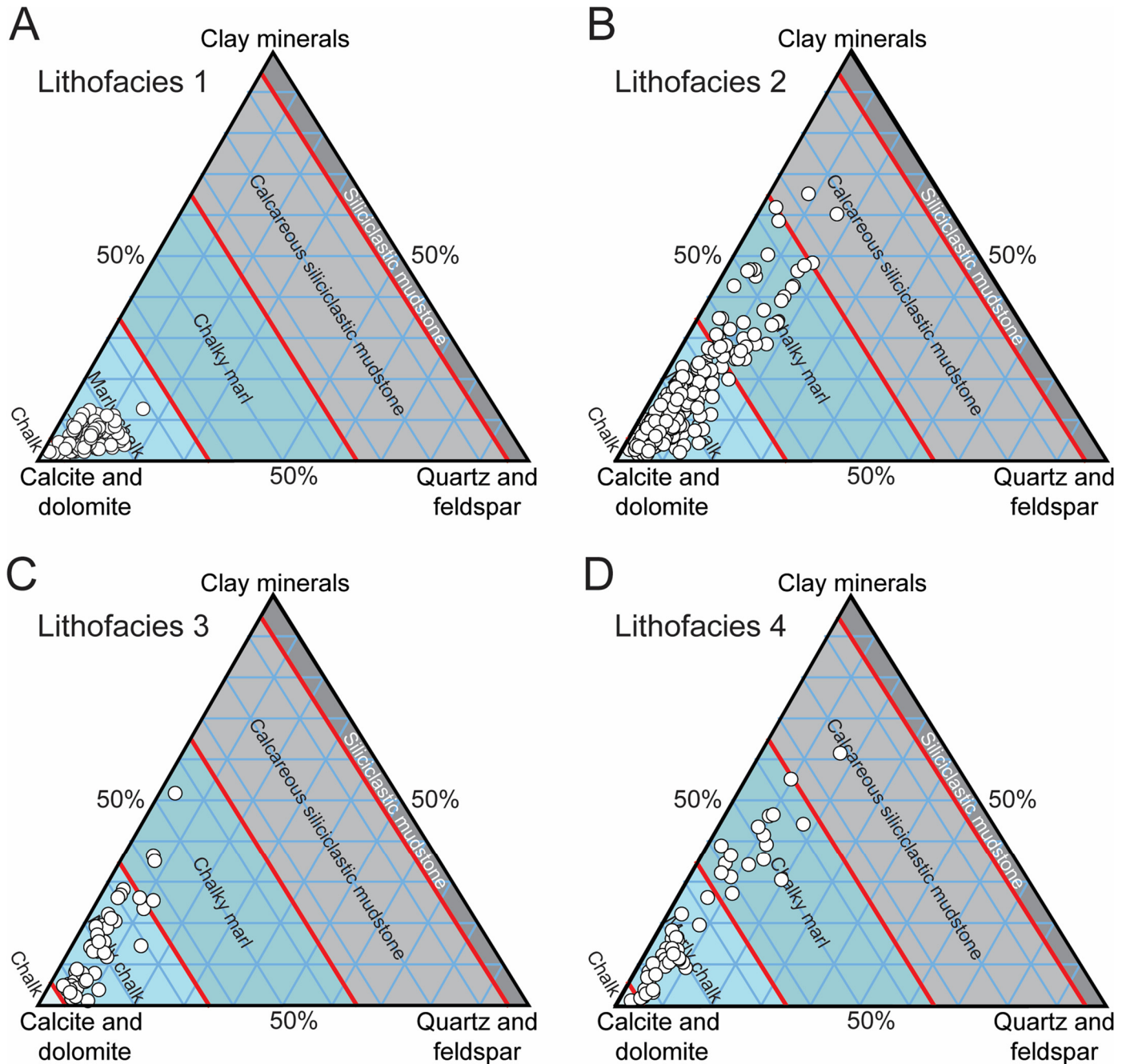

Figure 9. Mineralogy of samples by lithofacies. (A) Ternary diagram distribution for lithofacies 1. (B) Ternary diagram distribution for lithofacies 2. (C) Ternary diagram distribution for lithofacies 3. (D) Ternary diagram distribution for lithofacies 4.
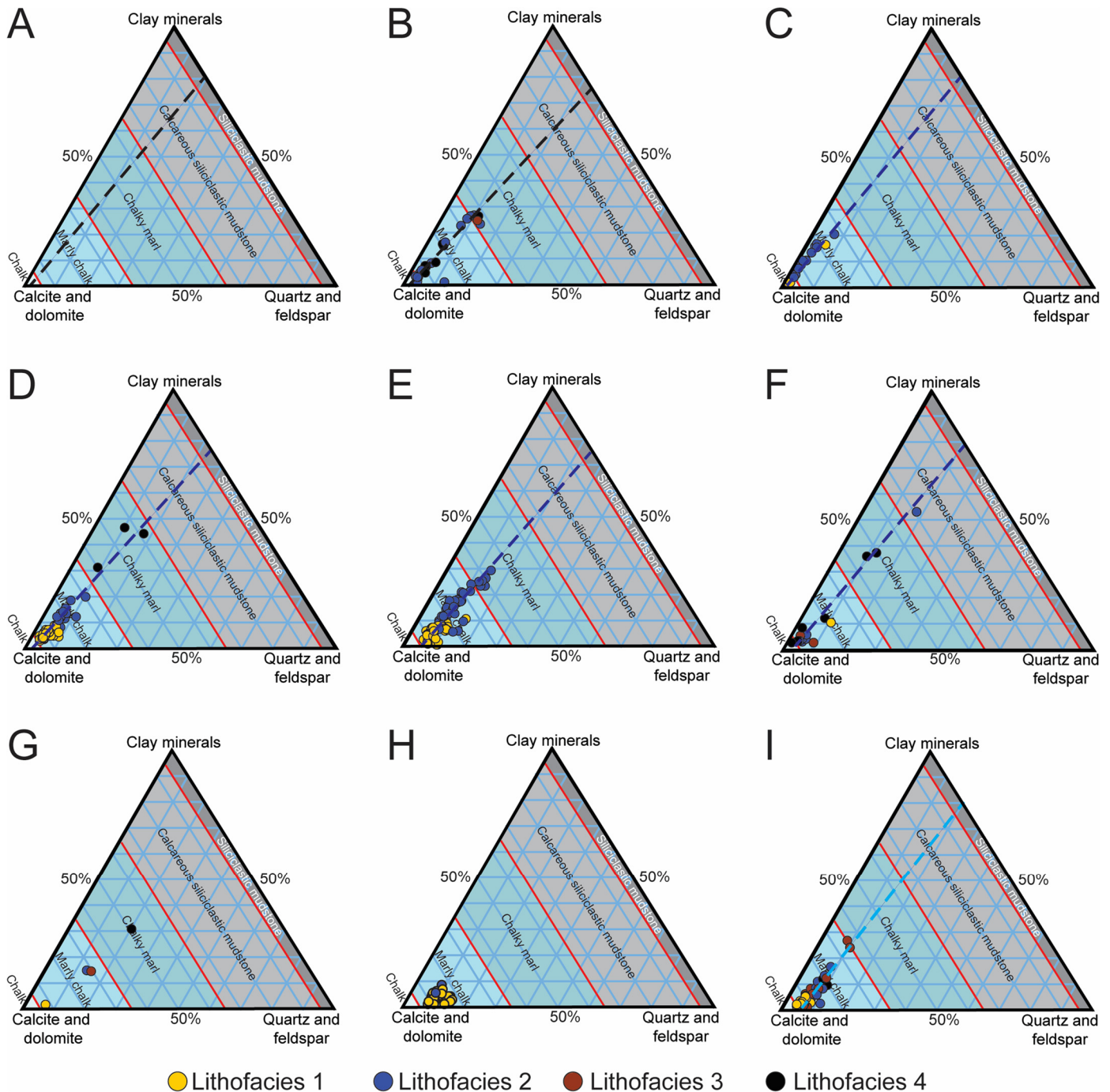
Figure 10. Ternary mineralogic plots by well. Trend lines are by eye. (A) Strata–X 1 Cinco Saus Creek, Maverick County, TX. (B) Getty Oil 1 Lloyd Hurt, La Salle County, TX. (C) Tesoro Petroleum 1 Valcher, Wilson County, TX. (D) Evergreen Oil 1 Vicker Olyn, Gonzales County, TX. (E) Trans Ocean Oil 2 HP Orts, Gonzales County, TX. (F) Devon 1 Medina, Dewitt County, TX. (G) Cities Service 1–B Ivy, Fayette County, TX. (H) Prairie Producing 1 Schautschick, Lee County, TX. (I) Prairie Producing 1 J. A. Smelley Et al, Lee County, TX.

REFERENCES CITED

Baldwin, O. C., and J. A. Adams, 1971, K^{40}/Ar^{40} ages of the alkalic igneous rocks of the Balcones Fault trend of Texas: Texas Journal of Science, v. 22, p. 223–231.

Barker, D. S., and K. P. Young, 1979, A marine Cretaceous nepheline basanite volcano at Austin, Texas: Texas Journal of Science, v. 31, p. 5–24.
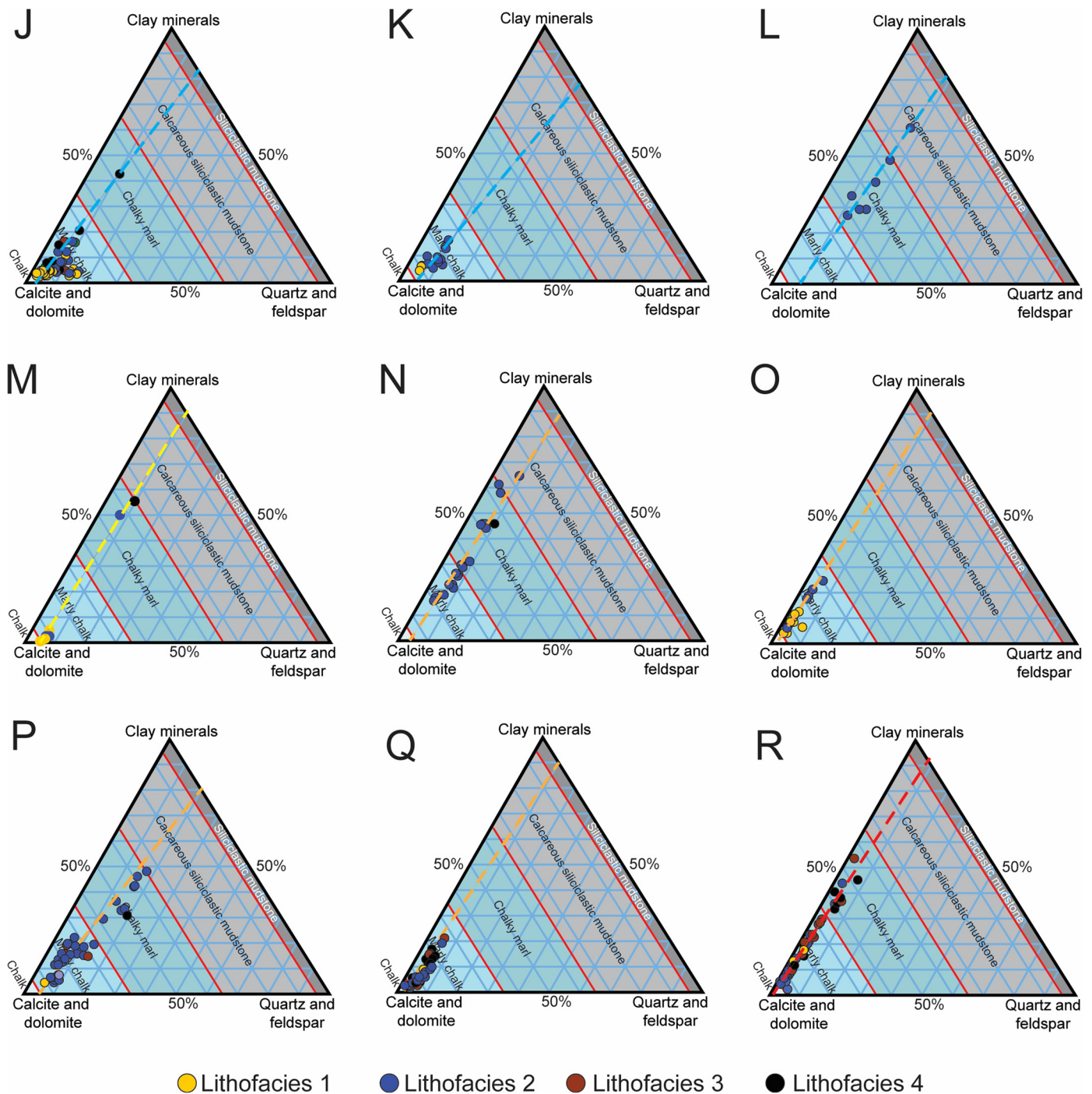
Figure 11. Ternary mineralogic plots by well. (J) Prairie Producing 1 Marburger, Lee County, TX. **(K)** Champlin Petroleum 1 Lancier Brinkman, Burleson County, TX. **(L)** Prairie Producing 1 Frances Restino, Roberson County, TX. **(M)** Shell 1 Southern Paper Mills, Polk County, TX. **(N)** Stonegate Production 1 Donner, Sabine Parish, LA. **(O)** Coffman 1 Cabra, Sabine Parish, LA. **(P)** ARCO 1 W Singletary, Beauregard Parish, LA. **(Q)** Cortex Energy C1 Musser Davis, Beauregard Parish, LA. **(R)** Marathon Oil 1 Robert Todd, West Feliciana Parish.

Chafetz, H. S., and A. Reid, 2000, Syndepositional shallow-water precipitation of glauconitic minerals: Sedimentary Geology, v. 136, p. 29–42, <https://doi.org/10.1016/S0037-0738(00)00082-8>.

Cobban, W., and K. McKinney, 2004, "Cretaceous seaway," Wikipedia: Appalachia (Mesozoic), <https://en.wikipedia.org/wiki/Appalachia_(Mesozoic)#/media/File:Cretaceous_seaway.png>.

Denne, R. A., R. E. Hinote, J. A. Breyer, T. H. Kosanke, J. A. Lees, N. Engelhardt-Moore, J. M. Spaw, and N. Tur, 2014, The Cenomanian-Turonian Eagle Ford Group of South Texas: Insights on timing and paleoceanographic conditions from geochemistry and micropaleontologic analyses: Palaeogeography, Palaeoclimatology, Palaeoecology, v. 413, p. 2–28, <https://doi.org/10.1016/j.palaeo.2014.05.029>.

Dennen, K. O., and P. C. Hackley, 2012, Definition of Greater Gulf Basin Lower Cretaceous and Upper Cretaceous lower Cenomanian Shale Gas Assessment Unit, United States Gulf of Mexico Basin onshore and state waters: American Association of Petroleum Geologists Search and Discovery Article 10429, Tulsa,
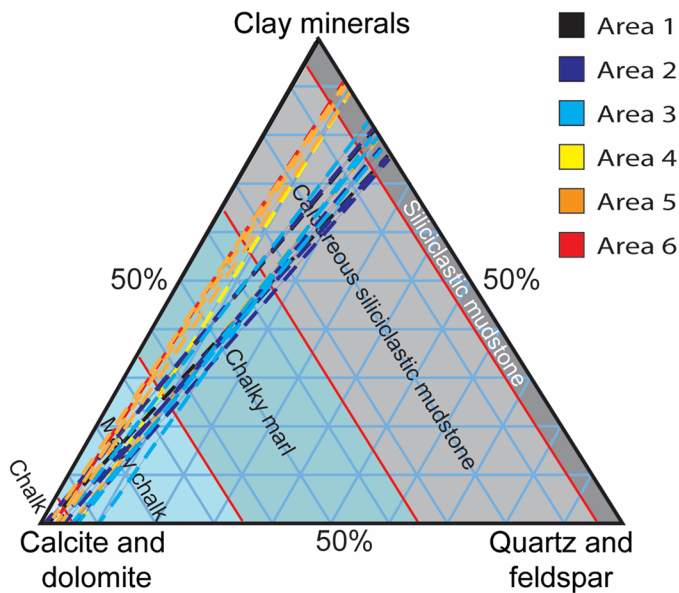
Figure 12. Mineralogic trend lines color coded by geographic area. See Figure 2 for geographic areas. Two populations are apparent.

Oklahoma, 37 p., <http://www.searchanddiscovery.com/pdfz/documents/2012/10429dennen/ndx_dennen.pdf.html>.

Ece, O. I., Z. Nakagawa, and P. A. Schroeder, 2003, Alteration of volcanic rocks and genesis of kaolin deposits in the Şile region, northern Istanbul, Turkey. I: Clay minerology: Clays and Clay Minerals, v. 51, p. 675–688, <https://doi.org/10.1346/CCMN.2003.0510610>.

Ewing, T. E., 2013, Stratigraphy of the Austin, Eagle Ford, and Anacacho formations and its influence on hydrocarbon resources, Pearsall Field area, South Texas: Gulf Coast Association of Geological Societies Transactions, v. 63, p. 213–225.

Ewing, T. E., and S. C. Caran, 1982, Late Cretaceous volcanism in South and Central Texas—Stratigraphic, structural, and seismic models: Gulf Coast Association of Geological Societies Transactions, v. 32, p. 137–145.

Fabricius, I. L., 2007, Chalk: Composition, diagenesis and physical properties: Bulletin of the Geological Society of Denmark, v. 55, p. 97–128.

Griffin, W. R., K. A. Foland, R. J. Stern, and M. I. Leybourne, 2010, Geochronology of bimodal alkaline volcanism in the Balcones Igneous Province, Texas: Implications for Cretaceous intraplate magmatism in the northern Gulf of Mexico magmatic zone: Journal of Geology, v. 118, p. 1–21, <https://doi.org/10.1086/648532>.

Jeans, C. V., R. J. Merriman, J. G. Mitchell, and D. J. Bland, 1982, Volcanic clays in the Cretaceous of southern England and Northern Ireland: Clay Minerals, v. 17, 105–156, <https://doi.org/10.1180/claymin.1982.017.1.10>.

Kok, J. F., E. J. R. Parteli, T. I. Michaels, and D. Bou Karam, 2012, The physics of wind-blown sand and dust: Reports on Progress in Physics, v. 75, 119 p., <https://doi.org/10.1088/0034-4885/75/10/106901>.

Locklair, R. E., and B. B. Sageman, 2008, Cyclostratigraphy of the Upper Cretaceous Niobrara Formation, Western Interior,

U.S.A.: A Coniacian-Santonian orbital timescale: Earth and Planetary Science Letters, v. 269, p. 540–553, <https://doi.org/10.1016/j.epsl.2008.03.021>.

Loucks, R. G., T. E. Larson, Y. Z. Zheng, C. K. Zahm, L. T. Ko, J. E. Sivil, S. Sheng, S. C. Ruppel, and W. A. Ambrose, in press, Geologic characterization of the type cored section for the Upper Cretaceous Austin Chalk Group in South Texas; a combination fractured and unconventional reservoir: American Association of Petroleum Geologists Bulletin.

Loucks, R. G., R. M. Reed, S. C. Ruppel, and D. M. Jarvie, 2009, Morphology, genesis, and distribution of nanometer-scale pores in siliceous mudstones of the Mississippian Barnett Shale: Journal of Sedimentary Research, v. 79, p. 848–861, <https://doi.org/10.2110/jsr.2009.092>.

Miggins, D. P., C. D. Blome, and D. V. Smith, 2002, Preliminary $^{40}Ar/^{39}Ar$ age constraints for the Uvalde igneous intrusions west of San Antonio, Texas: Geological Society of America Abstracts with Programs, v. 34, no. 6, p. 512, <https://gsa.confex.com/gsa/2002AM/webprogram/Paper46203.html>.

Miggins, D. P., C. D. Blome, and D. V. Smith, 2004, Preliminary $^{40}Ar/^{39}Ar$ geochronology of igneous intrusions from Uvalde County, Texas: Defining a more precise eruption history for the southern Balcones Volcanic Province: U.S. Geological Survey Open-File Report 2004–1031, 33 p., <https://doi.org/10.3133/ofr20041031>.

Phelps, R. M., C. Kerans, R. G. Loucks, R. O. B. P. Da Gama, J. Jeremiah, and D. Hull, 2013, Oceanographic and eustatic control of carbonate platform evolution and sequence stratigraphy on the Cretaceous (Valanginian-Campanian) passive margin, northern Gulf of Mexico: Sedimentology, v. 61, p. 461–496, <https://doi.org/10.1111/sed.12062>.

Pierce, J. D., S. C. Ruppel, H. Rowe, and D. F. Stockli, 2016, Zircon U–Pb geochronology and sources of volcanic ash beds in the Upper Cretaceous Eagle Ford Shale, South Texas: Gulf Coast Association of Geological Societies Journal, v. 5, p. 253–272, <https://gcags.org/Journal/2016.GCAGS.Journal/2016.GCAGS.Journal.v5.15.p253-274.Pierce.et.al.pdf>.

Raiswell, R., and D. E. Canfield, 1998, Sources of iron for pyrite formation in marine sediments: American Journal of Science, v. 298, p. 219–245, <https://doi.org/10.2475/ajs.298.3.219>.

Reading, H. G., and J. D. Collinson, 1996, Clastic coasts, *in* H. G. Reading, ed., Sedimentary environments: Processes, facies and stratigraphy: Blackwell Science, Oxford, U.K., p. 154–231.

Reed, R. M., J. E. Sivil, X. Sun, and S. C. Ruppel, 2019, Heterogeneity of microscale lithology and pore systems in an Upper Cretaceous Eagle Ford Group horizontal core, South Texas, U.S.A.: Gulf Coast Association of Geological Societies Journal, v. 8, p. 22–34, <https://www.gcags.org/Journal/2019.GCAGS.Journal/2019.GCAGS.Journal.v8.02.p22-34.Reed.et.al.pdf>.

Robertson, A., and P. Degnan, 1998, Significance of modern and ancient oceanic Mn–rich hydrothermal sediment, exemplified by Jurassic Mn–chert from Southern Greece, *in* R. A. Mills and K. Harrison, eds., Modern ocean floor processes and the geological record: Geological Society of London Special Publications, v. 148, p. 217–240, <https://doi.org/10.1144/GSL.SP.1998.148.01.12>.

Triplehorn, D. M., 1965, Origin and significance of glauconite in the geologic sequence: Tulsa Geological Society Digest, v. 33, p. 282–283.